Computing the absolute Gibbs free energy in atomistic simulations: Applications to defects in solids

Bingqing Cheng[*] and Michele Ceriotti

Laboratory of Computational Science and Modeling, Institute of Materials,
École Polytechnique Fédérale de Lausanne, 1015 Lausanne, Switzerland

The Gibbs free energy is the fundamental thermodynamic potential underlying the relative stability of different states of matter under constant-pressure conditions. However, computing this quantity from atomic-scale simulations is far from trivial, so the potential energy of a system is often used as a proxy. In this paper, we use a combination of thermodynamic integration methods to accurately evaluate the Gibbs free energies associated with defects in crystals, including the vacancy formation energy in bcc iron, and the stacking fault energy in fcc nickel, iron, and cobalt. We quantify the importance of entropic and anharmonic effects in determining the free energies of defects at high temperatures, and show that the potential energy approximation as well as the harmonic approximation may produce inaccurate or even qualitatively wrong results. Our calculations manifest the necessity to employ accurate free energy methods such as thermodynamic integration to estimate the stability of crystallographic defects at high temperatures.

I. INTRODUCTION

Knowledge of the Gibbs free energy is crucial in predicting the relative stability of different states of materials and molecules, and underlies a plethora of physical and chemical phenomena including phase diagrams, solubility, equilibrium concentration of defects, and so on. However, free energy calculations in atomistic simulations are often technically challenging and/or computationally demanding. For this reason, in many cases—particularly those involving solid phases—the potential energy of the local minimum configuration associated with a given state is used as a simple proxy, and at times a harmonic correction is also included as the entropic term.

One class of standard free energy techniques, such as metadynamics, umbrella sampling, and transition path sampling [1–3], relies on the concept that the phase space of a system can be divided into a number of states using a choice of reaction coordinates (or collective variables), and the free energy difference between two states can then be computed by sampling both states, as well as the transition paths that connect them.

Another class of free energy methods concentrates on computing the "absolute" free energy of a system by performing a thermodynamic integration (TI) [4–6]. The TI can be performed along a physical path, for example, along temperature or pressure, or via an unphysical path between the physical system and a reference system over a switching parameter λ. For the latter route, the parameterized Hamiltonian can be taken to be $\mathcal{H}(\lambda) = (1 - \lambda)\mathcal{H}_{\text{ref}} + \lambda\mathcal{H}$, where $\mathcal{H}$ is the actual Hamiltonian and $\mathcal{H}_{\text{ref}}$ is for the reference system with a known free energy. For example, the Helmoltz free energy of a crystal can be obtained by TI from an Einstein crystal, whose free energy can be expressed analytically, to the fully interacting system [6–10]. The Gibbs free energy of liquid water can be computed by following a thermodynamic path from a Lennard-Jones model to the real potential [11]. However, each TI route is associated with different complications, which have been extensively discussed in the literature, such as the singularity around $T = 0$ when integrating with respect to the system temperature [12], and the pathological divergence of $d\mathcal{H}(\lambda)/d\lambda$ that is often observed at the end points of the integral when switching between the real and the reference systems [5,7,13,14]. As such, in general, it is not trivial to find an optimal route for TI for a specific system.

The free energies associated with crystallographic defects (e.g., vacancies, dislocations, grain boundaries, surfaces, etc.) are extremely important in predicting the microstructures and the properties of crystalline materials. For example, the free energy of stacking faults is crucial in predicting the dislocation nucleation rate [15], the free energies associated with different surface reconstructions determine the surface phase diagram [16], grain boundary free energy affects the rate of boundary migration [17]. However, computing the free energies associated with the defects is a particularly challenging problem, which reveals many of the shortcomings of standard free energy methods. Determining a physical or a virtual transition path to introduce or destroy a defect inside a crystal is often complicated, ruling out techniques such as metadynamics or umbrella sampling. Thermodynamic integration over λ using a harmonic reference often leads to divergences at high temperatures, when diffusive and anharmonic behaviors become dominant [13]. Due to these difficulties in free energy estimations, the defect free energies are usually approximated by just the potential energy of defects or by harmonic approximations [18,19]. Recently, a number of studies have revealed significant temperature dependency of the stacking fault free energy due to entropic effects [15,20,21]. It has also been shown that vacancy formation energy at high temperatures is strongly

[*]bingqing.cheng@epfl.ch

by [4,24]

$$Q(N,V,T) = \frac{V^N}{\Lambda^{3N} N!} \int_{D(V)} d\mathbf{q} \exp\left[-\frac{U(\mathbf{q})}{k_B T}\right], \quad (1)$$

where the potential energy U is a function of the atomic coordinates $\mathbf{q} = \{\mathbf{q}_{1...N}\}$, $D(V)$ denotes the spatial domain defined by the containing volume [4], and $\Lambda = \sqrt{2\pi \hbar^2 / m k_B T}$ is the thermal de Broglie wavelength. The expression for the Helmholtz free energy of the system is thus

$$\begin{aligned} A(N,&V,T) \\ &= -k_B T \ln Q(N,V,T) \\ &= -k_B T \ln \frac{V^N}{\Lambda^{3N} N!} - k_B T \ln \int_{D(V)} d\mathbf{q} \exp\left[-\frac{U(\mathbf{q})}{k_B T}\right], \end{aligned}$$
$$(2)$$

where the first term in the last line is the free energy of an ideal gas. When the isothermal-isobaric (NPT) ensemble is used instead, the system can be characterized by the Gibbs free energy

$$\begin{aligned} G(N,&P,T) \\ &= -k_B T \ln \int dV \exp\left(-\frac{PV}{k_B T}\right) \exp\left[-\frac{A(N,V,T)}{k_B T}\right]. \end{aligned}$$
$$(3)$$

Computing directly the partition function for an arbitrary potential is impractical, and for this reason computational routes for evaluating A or G typically use a reference system for which the phase-space integral can be computed analytically, followed by one or more thermodynamic integration steps. Since TI does not require a smooth transformation of the atomic coordinates, but just the evaluation of free-energy derivatives as a function of a change in the thermodynamic conditions, many different paths can be used, and combined to obtain the most efficient protocol.

In the case of a solid system, which is the main focus of the present work, we found it effective to take a harmonic crystal reference, and follow the TI routes illustrated in Figure 1. In a nutshell, for evaluating the Helmholtz free energy A of a solid system, we propose to first integrate along λ between the harmonic and the real crystal and then do an integration with respect to the temperature T, which correspond to the yellow and the red arrows in Figure 1, respectively. To calculate the Gibbs free energy G of the system, we first obtain the Helmholtz free energy at a low temperature, switch from the NVT to the NPT ensemble, and finally do TI along the temperature T (the yellow, the blue, and the green arrows in Fig. 1). In the following, we discuss in detail how each step can be computed conveniently and efficiently.

Before we start the detailed discussion, note that in TI it is advantageous and often necessary to constrain the center of mass (CM) of the system. The Helmholtz free energy difference between the unconstrained and the constrained crystalline system under periodic boundary conditions can be expressed as [25]

$$\Delta A_{cm}(N,V,T) = -k_B T \left(\ln \frac{V}{N} + \frac{3}{2}\ln N + \ln \frac{1}{\Lambda^3}\right), \quad (4)$$
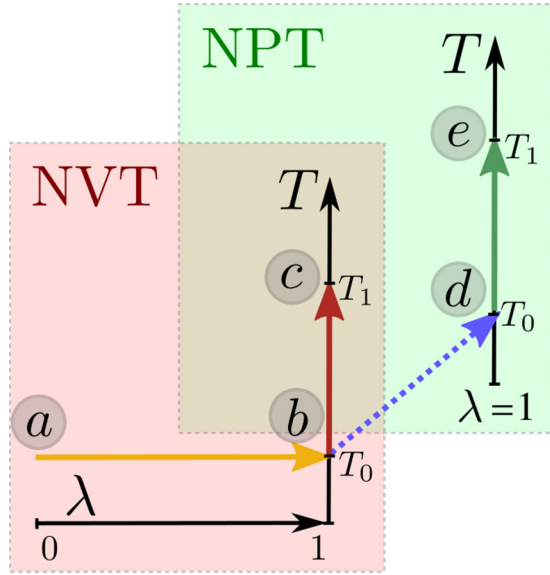

FIG. 1. An illustration of the different thermodynamic integration routes employed in the present paper. Under the canonical (NVT) ensemble, the yellow arrow indicates the switching between an harmonic reference system ($\lambda = 0$) and a real system ($\lambda = 1$), and the red arrow illustrates TI with respect to temperature. The dashed blue arrow shows the transformation between the Helmholtz free energy and the Gibbs free energy. The green arrow denotes TI over temperature under the isothermal-isobaric (NPT) ensemble.

affected by anharmonicity [22,23]. Overall, the community is becoming more aware that the accuracy of the prediction from the minimum potential energies may deteriorate at high temperatures.

In this paper, we use a combination of thermodynamic integration methods to compute the Gibbs free energies associated with crystallographic defects in solid systems. We discuss an optimized integration route (Fig. 1) that reduces the statistical error, and eliminates potential sources of divergence in the integration. We also introduce a direct connection between the TI routes under the canonical (NVT) ensemble and the isothermal-isobaric (NPT) ensemble, in order to freely transform between the Helmoltz free energy and the Gibbs free energy of a system. In addition, we incorporate several enhanced sampling methods and post-processing techniques to improve the overall statistical efficiency. Using this framework, we then calculate the free energy of a vacancy in bcc iron and the intrinsic stacking fault free energy in fcc nickel, iron and cobalt. We quantify the importance of entropic and anharmonic effects in these representative systems, demonstrating that they can significantly affect the free energies of defects in solids at high temperatures.

II. THEORY

The statistical-mechanical expression for the free energy of a system is closely related to the partition function, which in turn depends on the thermodynamic boundary conditions defining the ensemble. Under the canonical (NVT) ensemble, the partition function of a bulk system that has N *indistinguishable* particles and is contained in a volume V is given

which can be considered as a finite size effect. Therefore, when we perform TI, we focus solely on systems with fixed CM, and at the end of the calculation the term ΔA_{CM} can be added to retrieve the free energy of the unconstrained system, although at times the influence may be negligible. We will also discuss in more detail other finite-size effects in Sec. II F. In the other sections—since we will always work under the constant-number-of-particles framework in TI—we omit N when denoting thermodynamic states.

A. An absolute reference: the Helmoltz free energy of the Debye crystal

Strictly speaking, only the relative free energy of a system with respect to a reference can be defined without any ambiguity. The "absolute" free energy in this paper refers to the fact that the free energies of the chosen reference systems are analytic, and can be meaningfully compared between distinct reference systems including those that contain different numbers of particles.

A harmonically-coupled crystal of N atoms with a constrained center of mass constitutes a convenient reference system for a solid (point a in Fig. 1). Taking the phonon frequency for the crystal to be $\{\omega_{i=1,...,3N-3}\}$,[1] one can obtain an expression for the classical free energy of such a Debye crystal at the temperature T_0:

$$A_h(V,T_0) = k_B T_0 \sum_{i=1}^{3N-3} \ln \frac{\hbar\omega_i}{k_B T_0}. \qquad (5)$$

Note that from the standpoint of performing thermodynamic integration, the reference can be any harmonic crystal that has the same number of particles as the real system. For instance, one could even take a reference in which all particles are independently coupled to the lattice sites with a constant spring term (i.e., an Einstein crystal) [6,7,26]. However, for better statistical efficiency, it is better to choose a reference harmonic crystal that has the same frequency modes and equilibrium configuration as the real crystal, both of which can be determined for example via local energy minimization followed by a diagonalization of the Hessian matrix [27].

B. The Helmoltz free energy of an anharmonic crystal

Starting from a reference crystal (a) with a known free energy, one can obtain the Helmholtz free energy of the real crystal (b) using thermodynamic integration in the NVT ensemble, as indicated by the yellow arrow in Fig. 1 using a parameter λ to perform the switch between the harmonic Hamiltonian $\mathcal{H}_h$ and the actual Hamiltonian $\mathcal{H}$. In practice, one should run multiple simulations with the Hamiltonian $\mathcal{H}(\lambda) = (1-\lambda)\mathcal{H}_h + \lambda\mathcal{H}$ at different values of λ, so as to switch between the harmonic Hamiltonian $\mathcal{H}_h$ and the actual Hamiltonian $\mathcal{H}$ [7]. The free energy of the real system with a

fixed CM can then be evaluated using

$$A(V,T_0) - A_h(V,T_0) = \int_0^1 d\lambda \langle U - U_h \rangle_{V,T_0,\lambda}, \qquad (6)$$

where $\langle ... \rangle_{V,T_0,\lambda}$ denotes the ensemble average over NVT simulations using the Hamiltonian $H(\lambda)$.

In practice, to avoid severe statistical inefficiencies and singularities in the integral, one should perform this step at a low temperature T_0 when the system is quasiharmonic and when diffusive or rotational degrees of freedom are completely frozen. If T_0 is sufficiently low and the real and the reference systems are very similar, one also has the option to evaluate $A(V,T_0) - A_h(V,T_0)$ using the free energy perturbation method, eliminating the integration error altogether. One only needs to run simulations for the reference harmonic crystal, and obtain the free energy of the real system using

$$A(V,T_0) - A_h(V,T_0)$$
$$= -k_B T_0 \ln \left\langle \exp\left[-\frac{U-U_h}{k_B T_0}\right]\right\rangle_{V,T_0,\lambda=0}, \qquad (7)$$

where $\langle ... \rangle_{V,T_0,\lambda=0}$ denotes the ensemble average for the harmonic crystal at T_0 and V, and U and U_h denote the real and harmonic potentials, respectively. Note that in order to ensure the statistical efficiency of this perturbative approach, the standard deviation of $U - U_h$ has to be of the order of $k_B T_0$ [28].

C. The Helmholtz free energy as a function of temperature

Thermodynamic integration from a Debye crystal to the fully anharmonic potential tends to become very inefficient as the temperature increases. For this reason, it is often useful to perform a thermodynamic integration with respect to temperature from a low to a high temperature under the desired thermodynamic conditions. Let us start by discussing how to perform this step under the NVT ensemble, which is the process indicated by the red arrow (b to c) in Fig. 1. The Helmholtz free energy of a system that has N atoms and a fixed CM can be expressed by the well-known thermodynamic integration expression

$$\frac{A(V,T_1)}{k_B T_1} = \frac{A(V,T_0)}{k_B T_0} - \int_{T_0}^{T_1} \frac{\langle U \rangle_{V,T} + \langle K \rangle_{V,T}}{k_B T^2} dT, \qquad (8)$$

where $\langle U \rangle_{V,T}$ and $\langle K \rangle_{V,T}$ are the ensemble averages of the potential energy and the kinetic energy, respectively.

One way to improve the convergence of Eq. (8) is to consider that the ensemble average of the classical kinetic energy of a system that has N atoms and a fixed CM is analytic: $\langle K \rangle_{V,T} = (3N-3)k_B T/2$. Furthermore, one can also consider that if the potential was harmonic, also $\langle U \rangle$ would take the same value. Thus one can take

$$\langle \delta U \rangle_{V,T} = \langle U \rangle_{V,T} - A(V,0) - (3N-3)\frac{k_B T}{2} \qquad (9)$$

that measures the temperature-dependent anharmonic part of the potential energy. Note that $A(V,0) = \langle U \rangle_{V,0}$. After performing analytically some of the integrals, Eq. (8)

---

[1]The zero-frequency translational modes are excluded due to the constraint on CM.

becomes

$$
\frac{A(V,T_1)}{k_B T_1} = \frac{A(V,0)}{k_B T_1} + \frac{A(V,T_0) - A(V,0)}{k_B T_0}
$$
$$
- (3N - 3) \ln \frac{T_1}{T_0} - \int_{T_0}^{T_1} \frac{\langle \delta U \rangle_{V,T}}{k_B T^2} dT. \quad (10)
$$

In quasiharmonic systems, one can further reduce the variance of the integrand. One can use again the analytical expression for $\langle K \rangle_{V,T}$, together with the virial theorem, to write

$$
(3N - 3)\frac{k_B T}{2} = \langle K \rangle = -\frac{1}{2}\sum_{i=1}^{N} \langle \mathbf{F}_i \mathbf{q}_i \rangle. \quad (11)
$$

Here, $\mathbf{q}_i$ and $\mathbf{F}_i$ are the position of atom i and the force vector acting on it. Since the average force $\langle \mathbf{F}_i \rangle$ is zero, one can also add an arbitrary reference position $\hat{\mathbf{q}}_i$, and write [12,14]

$$
\langle \delta U \rangle_{V,T} = \left\langle U + \frac{1}{2}\sum_{i=1}^{N} \mathbf{F}_i(\mathbf{q}_i - \hat{\mathbf{q}}_i) \right\rangle_{V,T} - A(V,0). \quad (12)
$$

If the potential energy surface is perfectly harmonic, and if one takes $\hat{\mathbf{q}}_i$ equal to the equilibrium position of atom i, it is easy to verify that the virial term would cancel completely the fluctuations in the potential energy. Even if the potential is quasiharmonic, as long as it is not diffusive even at high temperatures, the use of the virial reference and Eq. (12) can substantially improve the statistical efficiency in the estimation of $\langle \delta U \rangle_{V,T}$. However, when the motion of atoms is strongly anharmonic or diffusive, an atom can start vibrating around a different equilibrium position, and in that case the statistical efficiency of the straightforward expression (9) is better.

Besides improving the convergence of each temperature window, one can try to improve the accuracy and the efficiency of the TI procedure by choosing wisely the discretization points or, equivalently, by performing a change of variables that yields a smoother integrand [29]. In this case, it is convenient to perform a change of variables that ensures that the statistical error in the integrand is roughly constant at all temperatures. Assuming the temperature dependence of the fluctuations in the anharmonic potential energy is similar to its harmonic counterpart, i.e., $\langle \delta U^2 \rangle_{V,T} - \langle \delta U \rangle_{V,T}^2 \sim T$, the required change of variable is $y = \ln(T/T_0)$, which transforms the integral into the form

$$
\int_{T_0}^{T_1} \frac{\langle \delta U \rangle_{V,T}}{T^2} dT = \int_{0}^{\ln(T_1/T_0)} \frac{\langle \delta U \rangle_{V,T_0 e^y}}{T_0 e^y} dy. \quad (13)
$$

In other words, one should select temperatures that are equally spaced in $\ln(T)$ in simulations. Coincidentally, this selection is also optimal for performing replica exchanges between the systems at different temperatures [30]—which should be done whenever possible as it will greatly benefit statistical convergence.

Another advantage of performing parallel tempering is that it requires sufficient overlap between adjacent replicas at temperatures T_i and T_{i+1}. Under these circumstances, $\langle U \rangle_{V,T}$ for $T_i < T < T_{i+1}$ can be evaluated via reweighting, such as

$$
\langle U \rangle_{V,T} = \frac{\left\langle U \exp\left[-\frac{U}{k_B}\left(\frac{1}{T} - \frac{1}{T_i}\right)\right]\right\rangle_{V,T_i}}{\left\langle \exp\left[-\frac{U}{k_B}\left(\frac{1}{T} - \frac{1}{T_i}\right)\right]\right\rangle_{V,T_i}}. \quad (14)
$$

The integral in Eq. (10) can thus be solved analytically to give an exact (within statistical uncertainty) expression for the contribution to the integral from the $[T_i, T_{i+1}]$ window:

$$
\frac{A(V,T_{i+1})}{k_B T_{i+1}} - \frac{A(V,T_i)}{k_B T_i}
$$
$$
= -\frac{3N-3}{2}\ln\frac{T_{i+1}}{T_i} - \ln\left\langle \exp\left[-\frac{U}{k_B}\left(\frac{1}{T_{i+1}} - \frac{1}{T_i}\right)\right]\right\rangle_{V,T_i}, \quad (15)
$$

which effectively turns the thermodynamic integration formalism into a sequence of free energy perturbations, eliminating completely the integration error.

D. From the Helmholtz free energy to the Gibbs free energy

More often than not, the isothermal-isobaric ensemble (NPT) provides a more natural framework to describe the thermodynamic conditions of real systems than the NVT ensemble. However, the harmonic crystal (a in Fig. 1) that was used as the absolute constant-volume reference in previous sections does not extend naturally to the NPT ensemble because its pressure is not well-defined (e.g., the Einstein crystal is a system of independent particles) [31]. As a result, it is not convenient to perform TI with respect to λ from the reference crystal to the real crystal under the NPT ensemble. One way to avoid NPT simulation involves performing multiple simulations at different constant volumes, and then computing the Gibbs free energy and the equilibrium volume of the system by evaluating explicitly the integral (3). This is often done using a harmonic expression for the free energy at the different volumes, leading to the so-called quasiharmonic approximation (QHA) [32,33]. Alternatively, the equilibrium volume can be computed by performing a single NPT simulation at the desired temperature, and then $A(\langle V \rangle_{P,T}, T)$ is used as a proxy for $G(P,T)$ [31]. In this section, we argue that the transformation between the Helmholtz free energy and the Gibbs free energy, which is the process marked by the dashed blue arrow in Figure 1, can be conducted rigorously. This process effectively allows us to convert at will between the two ensembles when performing thermodynamic integrations with respect to ensemble temperature.

The expression for the Gibbs free energy of a system as an integral over the Helmholtz free energy is given by Eq. (3). This expression can be combined with that for the distribution of volume fluctuations for the system under the NPT ensemble,

$$
\rho(V|P,T) = \frac{\exp\left(-\frac{PV}{k_B T}\right)\exp\left[-\frac{A(V,T)}{k_B T}\right]}{\int dV \exp\left(-\frac{PV}{k_B T}\right)\exp\left[-\frac{A(V,T)}{k_B T}\right]}, \quad (16)
$$

which is just the normalized probability of observing the system to have instantaneous volume V in a simulation under constant P and T. We can then write

$$
G(P,T) = A(V,T) + PV + k_B T \ln \rho(V|P,T), \quad (17)
$$

which is valid for arbitrary V.

In practice, one can run NPT simulations for a system and compute $\rho(V|P,T)$ just by accumulating the histogram of the instantaneous volume of the system. After that, one can select a volume V, preferably the one that maximizes $\rho(V|P,T)$ for

the sake of better statistical efficiency in the determination of $\rho(V|P,T)$, and compute $A(V,T)$ for the same system at that volume using the route a to b in Fig. 1. Finally, the Gibbs free energy can be obtained applying Eq. (17).

For a solid system, in order to avoid residual strain and elastic energy, one can vary the shape of the simulation cell instead of using a fixed shape in NPT simulations under a hydrostatic pressure [34]. To account for the degree of freedom associated with the variable cell, in this case, Eq. (17) should be modified to read

$$G(P,T) = A(\mathbf{h},T) + P\det(\mathbf{h}) + k_B T \ln\rho(\mathbf{h}|P,T), \quad (18)$$

where $\mathbf{h}$ is a matrix that represents the dimensions of a simulation cell, and $A(\mathbf{h},T)$ is the free energy of the system evaluated at constant cell dimensions.

E. The Gibbs free energy as a function of temperature

Having converted a harmonic-reference Helmoltz free-energy to a constant-pressure Gibbs free energy at a given temperature T_0, one can easily perform a thermodynamic integration over temperature in the NPT ensemble (a path indicated by the green arrow in Fig. 1). For a system with N atoms and a restricted CM, the expression reads

$$\frac{G(P,T_1)}{k_B T_1} = \frac{G(P,T_0)}{k_B T_0} - \int_{T_0}^{T_1} \frac{\langle H\rangle_{P,T}}{k_B T^2}dT, \quad (19)$$

where $\langle H\rangle_{P,T} = \langle U\rangle_{P,T} + (3N-3)\frac{k_B T}{2} + P\langle V\rangle_{P,T}$ is the enthalpy. Starting from this expression, one can apply all the techniques mentioned in Sec. II C, for example, one can take

$$\langle\delta H\rangle_{P,T} = \langle H\rangle_{P,T} - G(P,0) - (3N-3)\frac{k_B T}{2}, \quad (20)$$

where $G(P,0) = \langle U\rangle_{P,0} + P\langle V\rangle_{P,0}$. Doing the integration in Eq. (19) explicitly leaves

$$\frac{G(P,T_1)}{k_B T_1} = \frac{G(P,0)}{k_B T_1} + \frac{G(P,T_0) - G(P,0)}{k_B T_0}$$
$$- (3N-3)\ln\frac{T_1}{T_0} - \int_{T_0}^{T_1}\frac{\langle\delta H\rangle_{P,T}}{k_B T^2}dT. \quad (21)$$

In addition, one can also use the virial theorem [Eq. (11)], the change of variable in the integration [Eq. (13)], and parallel tempering to further accelerate the convergence. When performing parallel tempering, one can eliminate the thermodynamic integration error by using a free-energy perturbation to compute the increment of G between two replicas at temperatures T_{i+1} and T_i:

$$\frac{G(P,T_{i+1})}{k_B T_{i+1}} - \frac{G(P,T_i)}{k_B T_i}$$
$$= -\frac{3N-3}{2}\ln\frac{T_{i+1}}{T_i}$$
$$- \ln\left\langle\exp\left[-\frac{U+PV}{k_B}\left(\frac{1}{T_{i+1}} - \frac{1}{T_i}\right)\right]\right\rangle_{P,T_i}. \quad (22)$$

F. Finite size effects

Most of the time, one is interested in computing the free energy per atom of a bulk, infinite system, or the excess free energy of a defect in the dilute limit. An atomistic simulation, however, is inevitably restricted to a finite system size, which can result in deviations from the ideal case. Many of these finite-system-size effects have been documented in the literature. First of all, in the limit of small system size, the free energy of the system is not an extensive quantity. Taking the ideal gas part of the Helmholtz free energy $A_{id}(N,V,T) = -k_B T \ln\frac{V^N}{\Lambda^{3N}N!}$ in Eq. (2), for example, one can see that

$$\frac{A_{id}(N,V,T)}{Nk_B T} = 1 - \ln\frac{V}{N} + \ln\frac{1}{\Lambda^3} - \frac{\ln N}{2N} + \mathcal{O}\left(\frac{1}{N}\right) \quad (23)$$

using Stirling's formula. The leading $\ln N/N$ term is a well-documented finite size effect that reduces to zero in the thermodynamic limit [25,35]. The Gibbs free energy per atom $G(N,P,T)/N$ as well as $k_B T \ln\rho(V|P,T)/N$ in Eq. (16) also displays a similar dependence on $\ln N/N$. Constraining the center of mass of the system in simulations also introduces a nonextensive correction to the free energy,

$$\Delta A_{\rm cm}(N,V,T) = A(N,V,T) - A_{\rm cm}(N,V,T), \quad (24)$$

where $A_{\rm cm}$ denotes the Helmholtz free energy of the system with fixed center of mass [5,25]. Fortunately, it is easy to correct for this part, because the expression for $\Delta A_{\rm cm}$ in Eq. (4) is analytic and trivial to compute. More subtle sources of finite size effects come from the cutoff of potentials, and from the discretization of the vibrational phonon spectrum due to the size of the supercell in simulations [31]. To help with this issue, there are interpolation techniques that help accelerate the convergence of the computed phonon dispersion relation [36].

It is worth stressing that for system sizes that can be reached easily in simulations using empirical force fields, finite-size effects may not be significant. However, one should always be aware of their presence and check for system-size convergence, particularly in *ab initio* calculations where the number of atoms that can be simulated is highly restricted. To minimize the impact of finite-size effects one should always compare free energies between systems of similar sizes, to benefit for a (partial) error cancellation.

III. APPLICATION 1: VACANCY FREE ENERGY

A. Introduction

A vacancy is a type of point defects in a crystal, in which an atom is removed from one of the lattice sites. At any given temperature and pressure up to the solid-liquid coexistence line, an equilibrium concentration $\exp[-G_{\rm v}/k_B T]$ of vacancies exists, where $G_{\rm v}$ is the Gibbs free energy of a vacancy. Often, particularly in materials produced by fast quenching, a nonequilibrium concentration of vacancies can persist at low temperature, which can play an important role in technologically relevant solid-state transformations [37].

Several experimental techniques including positron annihilation and quenching can be used to characterize the vacancy formation energy. High-temperature experiments and data

analyses are, however, difficult [38]. As such, when interpreting experimental observations, it is often assumed that the equilibrium concentration of vacancies follows the Arrhenius law, and that the vacancy formation energy is constant across different temperatures [38]. However, molecular dynamics simulations suggest that the temperature dependence of the vacancy formation energy can be a complicated one [39].

B. System selection and simulation details

We studied a bcc iron system using a widely used EAM potential [40,41]. This potential was fitted with the bcc vacancy formation energy at 0 K but lacks a thermally stable fcc phase [40,42]. Iron exhibits phase transitions between bcc α-iron, fcc γ-iron, and a bcc δ phase when increasing the temperature at ambient pressure, which are largely due to the magnetism of the material [42]. Since the stabilization of the austenitic phase is due to quantum mechanical effects and this EAM potential does not reproduce it, we neglect the fcc phase in the present study, and performed the simulations considering a perfect bcc crystal (250 atoms) and a bcc crystal with a vacancy (249 atoms). In all the simulations, the centers of mass of the systems were constrained.

At high temperatures, the computation of the free energy of the crystal with a vacancy is particularly problematic using the integration over λ in Eq. (6) due to the onset of diffusion in simulations [13]. This difficulty is circumvented here as we performed the integration from the harmonic crystal to the real crystal at a low temperature $T_0 = 100$ K and at the equilibrium cell size (the yellow arrow in Fig. 1). This harmonic crystal has the same phonon modes and Hessian matrix as the real system [27,43]. Note that at this step the Helmholtz free energy of a crystal with a vacancy that sits at a fixed lattice site is computed, as the vacancy does not diffuse during the simulations at $T_0 = 100$ K. After that, we switched to the NPT ensemble (the blue arrow in Fig. 1), and ran simulations at different temperatures and zero hydrostatic pressure, using stochastic velocity re-scaling for temperature control and the anisotropic Nose-Hoover barostat to vary the dimensions of the orthorhombic periodic supercell [44,45]. During this step, we obtained the temperature dependence of the free energies using Eq. (19) (the green arrow in Fig. 1). At high temperatures, the vacancy does diffuse but diffusion does not change the values of $\langle \delta H \rangle_{P,T}$ compared with the case when the vacancy is fixed at one site, due to the translational symmetry of the lattice. As such, the Gibbs free energy of a crystal with a fixed vacancy was obtained after integration using Eq. (19). The absolute Gibbs free energies of the perfect bcc iron and the crystal with a fixed vacancy are included in the Supplemental Material [46], together with all the detailed procedures, the key data points, annotated input files and PYTHON notebooks for data analysis.

C. Gibbs free energy of a vacancy

The Gibbs free energy of a fixed vacancy in the crystal can be expressed as

$$G_{\text{v}} = G_{\text{vacancy}} - \frac{N_{\text{vacancy}}}{N_{\text{perfect}}} G_{\text{perfect}}. \qquad (25)$$
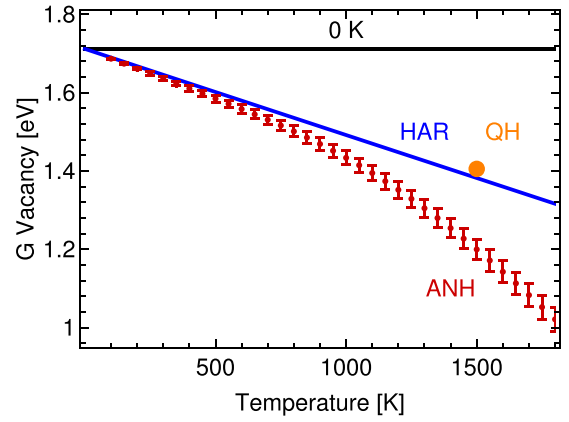

FIG. 2. The Gibbs free energy associated with a fixed vacancy in bcc iron estimated using the potential energy difference (PE) at 0 K, the harmonic approximation (HAR), and the thermodynamic integration method that considers anharmonicity (ANH). QH indicates the quasiharmonic approximation using the equilibrium configuration at 1500 K. Statistical uncertainties are indicated by the error bars.

We used three different methods to estimate this quantity—namely, a minimum-potential energy calculation, a harmonic free-energy estimate and the fully anharmonic TI—and plot the results in Fig. 2 as a function of temperature. Note that, for a given interatomic potential and within the statistical errors, the thermodynamic integration method gives access to the full Gibbs free energy, and can be considered as the ground truth. The other commonly used approximations, on the other hand, rest on different assumptions: the harmonic approximation method assumes that anharmonicity is negligible, while the minimum-potential energy method neglects both the anharmonicity and entropic contributions. By comparing the predictions from these approximation methods to the accurate values computed using thermodynamic integration, we can provide a representative benchmark of the accuracy of these approximations.

The difference between the predictions from the harmonic approximation and the TI is largely negligible at low temperatures, but becomes significant when the temperature approaches the melting point 1772 K for this EAM potential system [40]. To investigate whether this difference stems from a shift in the phonon spectra due to lattice expansion, or from anharmocity, we analyzed the vibrational modes $\{\omega'_{i=1,\dots,3N-3}\}$ using the equilibrium configuration of each system at 1500 K, computed the vacancy free energy under this quasiharmonic approximation, and plotted the result as the orange dot in Fig. 2. It can be seen that the harmonic contribution at 1500 K cannot explain the difference, and therefore the difference is mainly due to anharmonic effects.

IV. APPLICATION 2: STACKING FAULT FREE ENERGIES

A. Introduction

A stacking fault (SF) is a defect in the planar stacking sequence of atoms in a crystal. While the perfect stacking for fcc crystals along the [111] direction is $ABC|ABC|ABC|$, an intrinsic stacking fault changes the arrangement to $ABC|AB|ABC|$ as if one plane had been removed. The

stacking fault free energy (γ_{SF}) measures the free energy increase that is associated with the presence of the intrinsic stacking fault plane. The stacking fault free energy has a significant effect on the plastic deformation behavior of crystalline materials. For example, metals with a low γ_{SF} form more stacking faults and twins, and more extended partial dislocations which have reduced mobility [47–49]. Stacking faults also provide a strong barrier to dislocation gliding [47–49].

The magnitude of the stacking fault energy in fcc metals as well as how it varies with temperature has been extensively measured in experiments utilizing a variety of techniques including x-ray diffraction and observing extended dislocation nodes [50]. It is well-known that depending on the composition, the temperature dependence of the stacking fault free energy [$d\gamma_{SF}(T)/dT$] can exhibit a strongly positive or negative slope [50,51]. However, this temperature dependence is often neglected in the atomistic modelings, as quite often the potential energy difference caused by the stacking fault is used as a proxy to estimate γ_{SF}. In order to investigate the effect of entropy and anharmonic effects on $\gamma_{SF}(T)$, and to benchmark the accuracy of a number of commonly used approximations, we selected three representative metals that contain an fcc phase (nickel, iron, and cobalt) in their phase diagram.

B. System selections

fcc nickel has a high intrinsic stacking fault energy that has been estimated to be about 130 mJ/m^2 at room temperature decreasing to about 86 mJ/m^2 at 1333 K, corresponding to a slope $d\gamma_{SF}(T)/dT$ of about -0.04 mJ m^{-2} K^{-1} [51]. In our simulations described the Ni-Ni potential with a widely used EAM potential [41,52] that, however, predicts a considerably lower $\gamma_{SF} = 57$ mJ/m^2 for Ni at 0 K. Note that in general there is a quite substantial variability in the predictions of γ_{SF} from different EAM potentials for Ni [19].

The magnitude of the stacking fault energy dictates the mechanical properties of austenitic steels [53]. According to experimental measurements, γ_{SF} in various types of fcc iron based alloys ranges from about 10 to 100 mJ/m^2 at room temperature depending on the compositions [53]. In contrast, DFT calculations suggest that γ_{SF} in pure fcc iron and Fe-Mn alloys at 0 K are well below zero [54,55]. While of course pure fcc iron is not stable at room temperature, it is interesting to investigate whether anharmonic and entropic effects play a role in destabilizing stacking faults at finite temperature. To simulate pure fcc iron, we used the Ackland EAM potential [56], which predicts a negligible γ_{SF} at 0 K.

Cobalt is a transition metal whose equilibrium crystalline structure is hexagonal close packed (HCP) below 700 K and fcc above this temperature. Metastable fcc Co was found to exist at low temperatures [57]. Experimental measurements suggest that γ_{SF} in HCP cobalt increases from -30 to -18 mJ/m^2 at temperatures from 273 to 700 K, and γ_{SF} in fcc cobalt increases from 10mJ/m^2 to 20mJ/m^2 at temperatures from 700 to 1000 K with a positive temperature dependence around 0.03 mJ/m^{2}K [50]. In the simulations, we employed a newly developed EAM potential for Co that reliably reproduces many physical properties of both HCP and fcc cobalt, including the phase transition temperature [58].

Although we have found a number of good agreements between simulation predictions and experimental observations, we want to caution that the empirical EAM potentials may lack quantitative predictive power regarding the free energies of different structures and phases. For instance, different EAM potentials usually yield quite divergent estimates for the stacking fault energy, and a comprehensive comparison between them together with a few DFT results can be found in Ref. [19]. As such, the purpose of these simulations is to quantify the importance of entropic and anharmonic effects on γ_{SF} for representative metallic systems rather than attempting a direct prediction of experimental values, which would require a more reliable description of interatomic forces. Nevertheless, this work can be seen as a stepping stone in that direction, providing an optimized thermodynamic integration framework that can be combined with DFT or machine-learning potentials.

C. Simulation details

For each pure metal we selected (Ni, Fe, and Co), we performed the simulations of a perfect fcc crystal and of a fcc crystal with a stacking fault layer separately. The perfect fcc crystal used in simulations has 12 layers of {111} planes, and a total of $N_{perfect} = 1440$ atoms. The defective crystal has 11 layers with the stacking $ABC|ABC|AB|ABC|$, and a total of $N_{sf} = 1320$ atoms. We calculated separately the Gibbs free energy for both systems. The centers of the mass of the systems were constrained in all the simulations. All the detailed procedures and the key data points used in the calculations are included in the supplemental material [46], along with annotated input files and Python notebooks for data analysis for the case of Ni. In brief, we first computed the Helmholtz free energy of a real system at $T_0 = 90$ K by thermodynamic integration with respect to λ starting from a reference system using Eq. (6). The reference system is a harmonic crystal that has the same phonon modes and the Hessian matrix as the real system at the minimum potential energy [27,43], and the simulation cell is kept constant at the equilibrium size of the real system at 90 K. Afterwards, at temperatures that are equally spaced in $\ln(T)$, independent molecular dynamics simulations were performed under the NPT ensemble with zero external stress [44,45], in order to compute the anharmonic contributions $\langle \delta H \rangle_{P,T}$ and employ thermodynamic integration with respect to T using Eq. (21). We also found the use of the virial theorem to significantly reduce the fluctuations in the estimation of $\langle \delta H \rangle_{P,T}$ when we select $\hat{\mathbf{q}}$ to be the equilibrium position of the atoms in Eq. (12).

D. Stacking fault free energy estimations

The free energy excess ($\gamma_{SF} \times$ Area) that is associated with the stacking fault plane with a surface area equal to the cross section of the simulation supercell is just the difference between the free energies of a crystal with a stacking fault and a perfect bulk fcc crystal that have the same number of atoms:

$$\gamma_{SF} \times \text{Area} = G_{sf} - \frac{N_{sf}}{N_{perfect}} G_{perfect}. \qquad (26)$$

The results obtained for pure fcc Ni, Fe, and Co, using the three different methods to estimate $\gamma_{SF}(T)$, are compared with
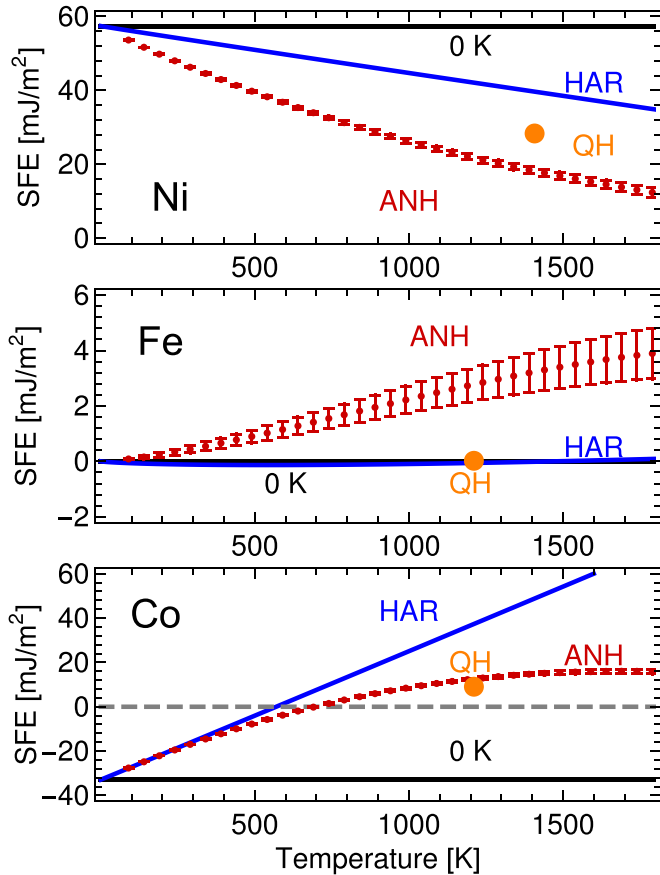
FIG. 3. The area-specific stacking fault free energy for pure fcc Ni, Fe, and Co as a function of temperature. The black lines are the estimations from potential energy difference at 0 K, the blue curves represent the harmonic approximation (HAR), and the red dots show the results from the thermodynamic integration method that considers anharmonicity (ANH). QH indicates the quasiharmonic approximation using the equilibrium configuration at the corresponding temperature and zero pressure. Statistical uncertainties are indicated by the error bars.

each other in Fig. 3. Let us reiterate that the shortcomings of the interatomic potential prevent a direction validation of different methods against experiments—which can be in themselves affected by large uncertainties. Our main objective here is to benchmark different approximations against the thermodynamic integration results, which are the correct free-energetic estimates for a given potential. For nickel, we found the estimations from just the potential energy at 0 K and the harmonic approximation are only accurate at very low temperatures. The prediction of the quasiharmonic approximation using the equilibrium configuration at 1408 K is more accurate than the harmonic approximation, but still differs by almost 50% from the fully anharmonic result. The inclusion of all the entropic and anharmonic effects dramatically decreases the stacking fault free energy at high temperatures, and the temperature dependence $d\gamma_{SF}(T)/dT$ is about -0.03 mJ/m^{2}K over a wide range of temperatures. This example on nickel highlights the peril of only using the 0 K potential energies to predict $\gamma_{SF}(T)$, which overestimates the magnitude of the stacking fault free energy by almost 300% at $T > 1200$ K. For fcc iron, the

potential energy method, the harmonic approximation and the quasiharmonic approximation all predict a negligible stacking fault energy at all temperatures. However, the anharmonic effects increase the stacking fault energy at higher temperatures, which was only captured by the thermodynamic integration method. This example suggests that anharmonicity can have a significant contribution on γ_{SF} at finite temperatures, and this contribution may help explain the discrepancy between the DFT calculations at 0 K [54,55] and the experimental measurements at higher temperatures [53]. For fcc cobalt, the stacking fault free energy is negative at temperatures below 700 K, indicating that an HCP to fcc phase transformation will happen at 700 K. This result is consistent with both the EAM potential employed and the experimental data [58]. The harmonic approximation also predicts the occurrence of such phase transition but fails to reproduce the correct transition temperature. The prediction of the quasiharmonic approximation is quite close to the thermodynamic integration result, indicating the influence from lattice expansion is probably the main culprit in the failure of the harmonic approximation method at high temperatures. Overall, $\gamma_{SF}(T)$ for fcc cobalt predicted from thermodynamic integration using the EAM potential [58] finds very good agreement with experiments [50], which is probably due to the fact that this potential has been specifically fitted to model the HCP to fcc transition.

V. CONCLUSIONS

The thermodynamic integration method, while being an exact and well-established free energy method widely used in statistical physics and chemical physics, is rarely applied in some of the fields of solid-state physics such as metallurgy. In the present study, we discuss how to construct an effective protocol to compute the fully anharmonic Gibbs free energy in solids, with a particular focus on defects in crystals.

In order to minimize the statistical error and to avoid numerical instabilities, we combined a number of thermodynamic integration routes, in a way that makes the best use of the similarity between a crystalline system and a harmonic Debye crystal at low temperatures, and at the same time fully take into account the anharmonic effects. Furthermore, we discuss how to convert between free energy values estimated under constant-volume and constant-pressure thermodynamic ensembles, and incorporate several techniques to enhance the efficiency and accuracy of free energy estimation. In Ref. [46], we have included all the input files, work-flows, and data analysis routines that were employed to produce the results discussed in the present paper, hoping to encourage and facilitate future efforts that aim to use thermodynamic integration methods to accurately predict the defect concentrations, phase diagrams, or any of the many materials properties that are determined by the Gibbs free energy.

The key merit of the thermodynamic integration method is that it does not rely on any approximations aside from the those underlying the interatomic potentials. For this reason, it can also be used as a benchmark for other approximation methods such as quasiharmonic approximations, self-consistent phonons [59–61], or the Greens function approach [62], that are often the only viable option when one uses expensive electronic-structure methods to compute more accurate

potentials. When needed, e.g., when the system contains light nuclei, it is also possible to include the oft-neglected quantum nuclear effects by using path-integral molecular dynamics and adding an extra TI route from the classical to the quantum mechanical system [9,63].

To demonstrate the importance of anharmonic and entropic effects in solids, we computed the free energy of a vacancy in bcc iron, and the stacking fault free energy of pure fcc nickel, iron, and cobalt. In all the cases, we found that both entropic and anharmonic effects play an important role in the free energy of defects at high temperatures. In the case of the stacking fault energies in iron and cobalt, the potential energy minima or the harmonic approximations yield qualitatively wrong results. The case of cobalt deserves particular attention, since the potential is fitted to reproduce the HCP/fcc phase transition, and can be expected to be accurate in describing the SFE. The full TI treatment predicts a change in sign of the SFE close to the experimental temperature of the phase transition, whereas the harmonic approximation underestimates the temperature by almost 200 K. Our findings suggest that, in order to accurately predict the stabilities of defect in crystals at high temperatures, not only a high quality interatomic potential is required, it is also necessary to employ accurate free energy methods that consider entropic and anharmonic effects. The thermodynamic integration framework that we discuss can be used together with a reliable potential surface to provide accurate predictions, or together with a computationally inexpensive empirical potential to gauge the significance of anharmonic effects in a system.

[1] A. Laio and M. Parrinello, Proc. Natl. Acad. Sci. USA **99**, 12562 (2002).

[2] G. M. Torrie and J. P. Valleau, J. Comput. Phys. **23**, 187 (1977).

[3] P. G. Bolhuis, D. Chandler, C. Dellago, and P. L. Geissler, Annu. Rev. Phys. Chem. **53**, 291 (2002).

[4] M. Tuckerman, *Statistical Mechanics: Theory and Molecular Simulation* (Oxford University Press, Oxford, UK, 2010).

[5] C. Vega, E. Sanz, J. Abascal, and E. Noya, J. Phys.: Condens. Matter **20**, 153101 (2008).

[6] L. M. Ghiringhelli, J. H. Los, E. J. Meijer, A. Fasolino, and D. Frenkel, Phys. Rev. Lett. **94**, 145701 (2005).

[7] J. M. Polson and D. Frenkel, J. Chem. Phys. **109**, 318 (1998).

[8] J. Anwar, D. Frenkel, and M. G. Noro, J. Chem. Phys. **118**, 728 (2003).

[9] M. Rossi, P. Gasparotto, and M. Ceriotti, Phys. Rev. Lett. **117**, 115702 (2016).

[10] L. Li, T. Totton, and D. Frenkel, J. Chem. Phys. **146**, 214110 (2017).

[11] E. Sanz, C. Vega, J. L. F. Abascal, and L. MacDowell, Phys. Rev. Lett. **92**, 255701 (2004).

[12] S. G. Moustafa, A. J. Schultz, and D. A. Kofke, Phys. Rev. E **92**, 043303 (2015).

[13] S. M. Foiles, Phys. Rev. B **49**, 14930 (1994).

[14] A. J. Schultz, S. G. Moustafa, W. Lin, S. J. Weinstein, and D. A. Kofke, J. Chem. Theory Comput. **12**, 1491 (2016).

[15] D. H. Warner and W. Curtin, Acta Mater. **57**, 4267 (2009).

[16] M. Valtiner, M. Todorova, G. Grundmeier, and J. Neugebauer, Phys. Rev. Lett. **103**, 065502 (2009).

[17] D. Turnbull, JOM **3**, 661 (1951).

[18] R. LeSar, R. Najafabadi, and D. J. Srolovitz, Phys. Rev. Lett. **63**, 624 (1989).

[19] J. A. Zimmerman, H. Gao, and F. F. Abraham, Modell. Simul. Mater. Sci. Eng. **8**, 103 (2000).

[20] S. Ryu, K. Kang, and W. Cai, Proc. Natl. Acad. Sci. USA **108**, 5174 (2011).

[21] W. K. Kim and E. B. Tadmor, Phys. Rev. Lett. **112**, 105501 (2014).

[22] B. Grabowski, L. Ismer, T. Hickel, and J. Neugebauer, Phys. Rev. B **79**, 134106 (2009).

[23] A. Glensk, B. Grabowski, T. Hickel, and J. Neugebauer, Phys. Rev. X **4**, 011018 (2014).

[24] M. P. Allen and D. J. Tildesley, *Computer Simulation in Chemical Physics* (Springer Science & Business Media, Dordrecht, Netherland, 2012), Vol. 397.

[25] J. M. Polson, E. Trizac, S. Pronk, and D. Frenkel, J. Chem. Phys. **112**, 5339 (2000).

[26] E. G. Noya, M. Conde, and C. Vega, J. Chem. Phys. **129**, 104704 (2008).

[27] P. Y. Ayala and H. B. Schlegel, J. Chem. Phys. **108**, 2314 (1998).

[28] M. Ceriotti, G. A. Brain, O. Riordan, and D. E. Manolopoulos, Proc. R. Soc. A **468**, 2 (2011).

[29] M. Ceriotti and T. E. Markland, J. Chem. Phys. **138**, 014112 (2013).

[30] D. J. Earl and M. W. Deem, Phys. Chem. Chem. Phys. **7**, 3910 (2005).

[31] R. Freitas, M. Asta, and M. de Koning, Comput. Mater. Sci. **112**, 333 (2016).

[32] J. Xie, S. de Gironcoli, S. Baroni, and M. Scheffler, Phys. Rev. B **59**, 965 (1999).

[33] R. Ramírez, N. Neuerburg, M.-V. Fernández-Serra, and C. Herrero, J. Chem. Phys. **137**, 044502 (2012).

[34] M. Parrinello and A. Rahman, J. Appl. Phys. **52**, 7182 (1981).

[35] W. G. Hoover, J. Chem. Phys. **49**, 1981 (1968).

[36] P. Giannozzi, S. de Gironcoli, P. Pavone, and S. Baroni, Phys. Rev. B **43**, 7231 (1991).

[37] S. Pogatscher, H. Antrekowitsch, M. Werinos, F. Moszner, S. S. A. Gerstl, M. F. Francis, W. A. Curtin, J. F. Löffler, and P. J. Uggowitzer, Phys. Rev. Lett. **112**, 225701 (2014).

[38] A. Seeger, Phys. Status Solidi A **167**, 289 (1998).

[39] M. I. Mendelev and B. S. Bokstein, Philos. Mag. **90**, 637 (2010).

[40] M. Mendelev, S. Han, D. Srolovitz, G. Ackland, D. Sun, and M. Asta, Philos. Mag. **83**, 3977 (2003).

[41] G. Bonny, R. C. Pasianot, N. Castin, and L. Malerba, Philos. Mag. **89**, 3531 (2009).

[42] C. Engin, L. Sandoval, and H. M. Urbassek, Modell. Simul. Mater. Sci. Eng. **16**, 035005 (2008).

[43] M. Ceriotti, J. More, and D. E. Manolopoulos, Comput. Phys. Commun. **185**, 1019 (2014).

[44] G. Bussi, D. Donadio, and M. Parrinello, J. Chem. Phys. **126**, 014101 (2007).

[45] S. Plimpton, J. Comp. Phys. **117**, 1 (1995).

[46] See Supplemental Material at http://link.aps.org/supplemental/ 10.1103/PhysRevB.97.054102 for detailed procedures of the thermodynamic integration method, key data points, annotated input files and PYTHON notebooks for data analysis.

[47] S. Allain, J.-P. Chateau, O. Bouaziz, S. Migot, and N. Guelton, Mater. Sci. Eng. A **387**, 158 (2004).

[48] H. Van Swygenhoven, P. Derlet, and A. Frøseth, Nat. Mater. **3**, 399 (2004).

[49] V. Yamakov, D. Wolf, S. Phillpot, A. Mukherjee, and H. Gleiter, Nat. Mater. **3**, 43 (2004).

[50] P. Gallagher, Metall. Trans. **1**, 2429 (1970).

[51] L. Murr, Scr. Metall. **6**, 203 (1972).

[52] A. F. Voter and S. P. Chen, MRS Online Proceedings Library Archive **82**, 175 (1986).

[53] R. Schramm and R. Reed, Metall. Mater. Trans. A **6**, 1345 (1975).

[54] I. Bleskov, T. Hickel, J. Neugebauer, and A. Ruban, Phys. Rev. B **93**, 214115 (2016).

[55] A. Reyes-Huamantinco, P. Puschnig, C. Ambrosch-Draxl, O. E. Peil, and A. V. Ruban, Phys. Rev. B **86**, 060201 (2012).

[56] G. Ackland, D. Bacon, A. Calder, and T. Harry, Philos. Mag. A **75**, 713 (1997).

[57] G. R. Harp, R. F. C. Farrow, D. Weller, T. A. Rabedeau, and R. F. Marks, Phys. Rev. B **48**, 17538 (1993).

[58] G. P. Pun and Y. Mishin, Phys. Rev. B **86**, 134116 (2012).

[59] D. Hooton, Philos. Mag. **46**, 422 (1955).

[60] S. E. Brown, I. Georgescu, and V. A. Mandelshtam, J. Chem. Phys. **138**, 044317 (2013).

[61] I. Errea, M. Calandra, and F. Mauri, Phys. Rev. B **89**, 064302 (2014).

[62] C. Campaná and M. H. Müser, Phys. Rev. B **74**, 075420 (2006).

[63] M. Rossi, W. Fang, and A. Michaelides, J. Phys. Chem. Lett. **6**, 4233 (2015).